

# Analysis of Log-amplitude Saturation of Noise Emission from a Loudspeaker in a Wind Turbine Nacelle

**Bertagnolio, F.; Fischer, A.; Shen, W.Z.; Vignaroli, A.; Hansen, K.S.; Hansen, P.; Søndergaard, L.S.**

*Publication date:*
2020

*Document Version*
Publisher's PDF, also known as Version of record

# ANALYSIS OF LOG-AMPLITUDE SATURATION OF NOISE EMISSION FROM A LOUDSPEAKER ON A WIND TURBINE NACELLE

**F. Bertagnolio**[1] **A. Fischer**[1] **W.Z. Shen**[1]
**A. Vignaroli**[1] **K.S. Hansen**[1] **P. Hansen**[1] **L.S. Søndergaard**[2]
[1] DTU Wind Energy, Denmark
[2] FORCE Technology, Denmark
frba@dtu.dk

## ABSTRACT

This work is concerned with the analysis of log-amplitude fluctuations, and their saturation at large distances, using loudspeaker broadband noise emissions. An experiment is conducted outdoor with a loudspeaker on a wind turbine nacelle at 109 m height and a row of microphones extends up to 1278 m from the loudspeaker. The measured saturation length presents a similar trend than a theoretical result for tonal noise and spherical waves, but there are large quantitative discrepancies.

## 1. INTRODUCTION

It is a known phenomenon that log-amplitude fluctuations from a tonal noise source do saturate (i.e. reach an upper limit) at a certain distance from the source in a turbulent medium such as the atmosphere [1]. However, there are much less available measurements or theoretical works for broadband noise, at least in the context of atmospheric noise propagation and wind turbine noise. Note that this phenomenon should be included in auralization techniques in order to obtain realistic audio simulations of noise sources at large distances [2].

In the present work, measurements of loudspeaker broadband noise emissions are conducted outdoor. The loudspeaker is located on the nacelle of a wind turbine to simulate wind turbine noise with a controlled noise source, and microphones are located near the ground from close to the turbine to the far-field. The experimental set-up and data processing is explained in the next two sections. The analysis of the results is conducted in Section 3, where experimental data are compared with the tonal noise and spherical waves theory.

## 2. EXPERIMENTAL SET-UP

An Electro-Voice ZLX loudspeaker is placed at the back of a nacelle of a wind turbine (see picture in Fig. 1). It is orientated such that it is pointing toward a line of 8 microphones. An aerial view of the microphone positions is provided in Fig. 2 (not including the microphones the farthest away Mic.10, see below). The first one is on the ground at standard IEC position from the wind turbine, while the remaining ones are on tripods located at either 1.2 or 1.5 m above the ground. The distances of each microphone to the loudspeaker position are reported in Table 1. Note that the numbering of the loudspeakers is not incremental because additional microphones (not used in the present analysis) were present during the campaign. A picture of the test site taken from Mic.8 position is displayed in Fig. 3. In addition, a microphone (denoted as Mic.0) is attached to the loudspeaker to more accurately evaluate the noise source, i.e. the loudspeaker (see Fig. 1). Finally, a met mast located near the turbine and equipped with various sensors is used to monitor wind conditions up to hub height.

**Figure 1**. Loudspeaker mounted on the back of the turbine nacelle seen from the ground.

The loudspeaker is iteratively activated with a sequence of white noise signals over successive 1/1 octave frequency bands consisting of those centered at 125 Hz, 250 Hz, 500 Hz, 1000 Hz and 2000 Hz, as well as an individual white noise signal over a larger frequency band ranging from 88 Hz to 2840 Hz (i.e. covering all previous 1/1 octave frequency bands). Each individual noise activation


**Figure 2**. Aerial view of microphone positions along the line (excluding Mic.10 which is positioned further away from the turbine than Mic.9 along the line).

**Figure 3**. Test site seen from Mic.8 with wind turbine in the background.

period lasts for 1 minute and they are separated by 20 s of silence.

A sample time-series of a 10 mins sequence starting and finishing by a large frequency band white noise is displayed in Fig. 4, displaying both non-weighted and A-weighted $L_{eq,\,1/8\,\mathrm{s}}$ (excluding the loudspeaker microphone Mic.0 for the latter case) recorded at all microphones. It can be observed on the Mic.0 signal that the loudspeaker contains an internal control system to reduce the power output, resulting in some activation periods starting with a few seconds of unsteady power output. The large frequency band white noise does not appear to stabilize. The figure also shows that the signal-to-noise ratio is quite high, even at the farthest away Mic.10, for the high frequency 1/1 octave band emissions by looking at A-weighted sound pressure level time-series.

The microphones are equipped with primary and secondary wind screen in all cases and correction for insertion losses are included in the results shown later in this

| Microphone number $j$ | Distance from loudspeaker $x_j$ [m] |
|---|---|
| Mic.0 | 1.35 |
| Mic.1 | 197 |
| Mic.4 | 393 |
| Mic.5 | 591 |
| Mic.6 | 714 |
| Mic.7 | 861 |
| Mic.8 | 985 |
| Mic.9 | 1178 |
| Mic.10 | 1278 |

**Table 1**. Position of microphones relative to loudspeaker.

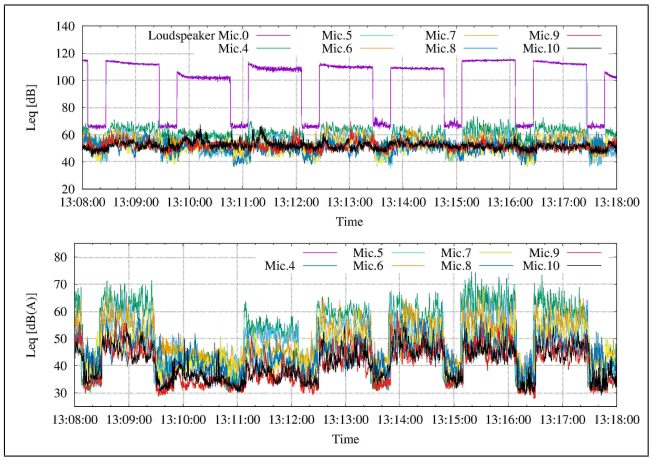


**Figure 4**. Time-series of sound pressure levels at all microphone for a sequence of 10 mins (Top: Non-weighted $L_{eq}$, Bottom: A-weighted $L_{eq}$ excluding Mic.0 at loudspeaker position).

paper. The acquisition of the data is performed with 2 separate PXI systems that can sample the microphone signals at 25600 Hz, and 3 hard-disk recorders sampling at 51200 Hz for Mics.4, 9 and 10.

## 3. DATA PROCESSING

The data are processed as follows. The exact time of the noise sequence activation starts and ends are evaluated using Mic.0. Then, the speed of sound is accounted for to allow the sound waves to reach the microphone the farthest away (i.e. Mic.10), and the sequence starting times are increased so that all microphones do record the loudspeaker noise. The unsteady power output starting periods are also removed from the analyzed activation periods (see previous section) further increasing the above actual starting times of the data included in the analysis. For the large frequency band white noise activation periods which amplitude appears to decrease linearly in time (see Fig. 4), the log-amplitude time-series are detrended before conducting the statistical analysis below.

For each microphone $j$, the remaining of these time-series when the loudspeaker is activated are splitted into $N$ sub-series of identical length equal to 1/16$^{\text{th}}$ of a second indexed $i$. The latter are Fourier transformed to obtain both

their amplitude $A_i(f,x_j)$ and phase $\Phi_i(f,x_j)$ $(i=1,N)$, where $f$ are the discrete frequencies of the Fourier transform. Then, the average values for the amplitude and phase are defined as:

$$\overline{A}(f,x_j) = \frac{1}{N}\sum_{i=1}^{N} A_i(f,x_j) \quad \text{and}$$

$$\overline{\Phi}(f,x_j) = \frac{1}{N}\sum_{i=1}^{N} \Phi_i(f,x_j) \quad (1)$$

according to Daigle *et al* [1]. Note that the phase has been unwrapped before conducting the present calculations. The log-amplitude for each sub-series is then defined as:

$$\overline{\chi}(f,x_j) = \ln\left(A_i(f,x_j)/\overline{A}(f,x_j)\right) \quad (2)$$

and variances as:

$$\langle\chi^2\rangle(f,x_j) = \frac{1}{N}\sum_{i=1}^{N}\left(\overline{\chi}(f,x_j)\right)^2 \quad \text{and}$$

$$\langle S^2\rangle(f,x_j) = \frac{1}{N}\sum_{i=1}^{N}\left(\Phi_i(f,x_j) - \overline{\Phi}(f,x_j)\right)^2 \quad (3)$$

for log-amplitude and phase, respectively. Note that Daigle *et al* [1] use a more advanced formula for the phase variance, but it did not change the results in our case.

The calculation of average values and variances for each microphone uses sub-series from 4 different successive activation periods of the same type. Thus, for a given 1/1 octave frequency band the data are collected over a time interval of approximately 40 mins for each individual activation period, but separated by 8 mins for identical activation types, resulting in slightly more than 3 mins of analyzed data in total.

## 4. RESULTS

### 4.1 Log-amplitude and phase fluctuations

The log-amplitude and phase variances as calculated in Eq. (3) for the various 1/1 octave frequency band activation periods are displayed in Figs. 5 to 9 for all microphones as a function of their distance from the loudspeaker, and frequency for each discrete frequency of the Fourier transform (see previous section).

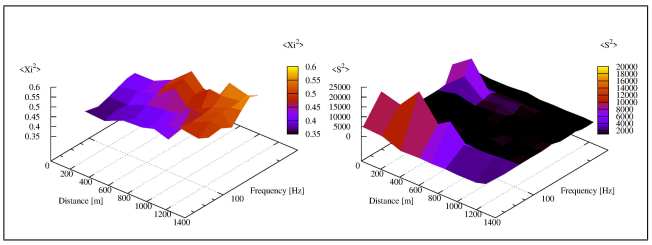


**Figure 5**. Log-amplitude and phase variances for 125 Hz 1/1 octave band emission.

It can be seen that the log-amplitude variance does saturate at some distance from the microphones, although the saturation length is clearly dependent on the considered frequency. It is also noted that this variance appears to actually slightly decrease at the microphones the farthest (at least for 1/1 octave frequency band than 250 Hz). It is attributed to the fact that at these distances the noise signal strength becomes very weak.

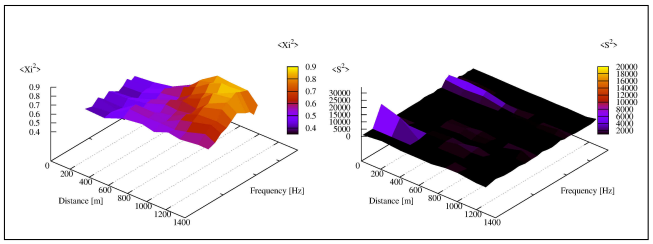


**Figure 6**. Log-amplitude and phase variances for 250 Hz 1/1 octave band emission.

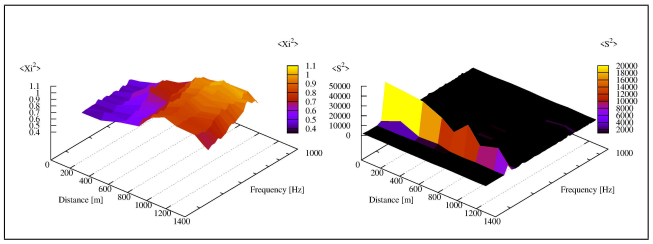


**Figure 7**. Log-amplitude and phase variances for 500 Hz 1/1 octave band emission.

As for the phase, it appears that its variance is only measurable at the frequency edges of the 1/1 octave frequency band emissions and appears to decrease as a function of distance. This phenomenon is not understood so far.

The background noise (i.e. the ambient noise at the microphones added on top of the loudspeaker noise immission levels) has certainly an impact on the accuracy of the results. Since background noise cannot be removed from the measurements and performing the analysis of Section 3 on background noise only does not really make sense, the variability of the results is looked at instead. Note that it can well be that the observed variability is caused by turbulence intermittency rather than background noise itself. Fig. 10 displays the results for the individual 4 sub-series mentioned at the end of Section 3 which are used to generate the plot of the log-amplitude variance in Fig. 7 on the left side (only the 1/1 octave band emission centered at 500 Hz is considered here). It can be seen that some variability does exist. Nevertheless, the procedure of looking at several time periods should average out background noise and/or turbulence intermittency as the comparison of Figs. 7 and 10 suggests.

### 4.2 Saturation length

According to the theoretical approach by Wenzel [3] for tonal noise, the distance of saturation is given by:

$$r_s = 1/\left(2\,\langle\mu^2\rangle k^2 L\right) \quad (4)$$

where $k$ is the considered wave number, $L$ is a measure of the scale of turbulence and $\mu$ is the fluctuating part of the

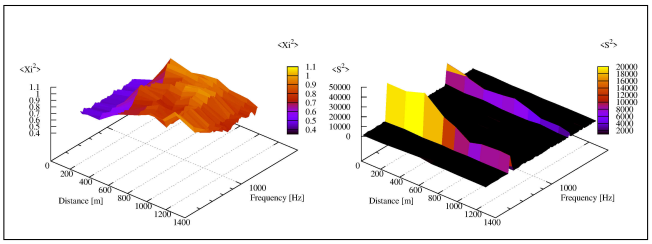


**Figure 8**. Log-amplitude and phase variances for 1000 Hz 1/1 octave band emission.

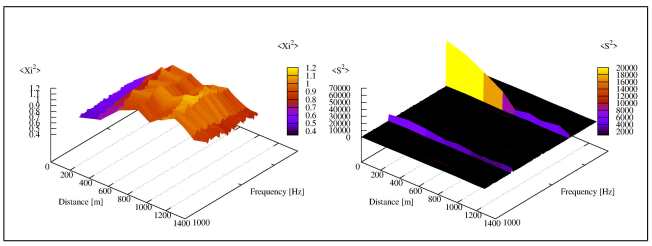


**Figure 9**. Log-amplitude and phase variances for 2000 Hz 1/1 octave band emission.

refractive acoustical index $n$ such that $n = 1 + \mu$, where $\mu \ll 1$.

The wind speed is measured at the met mast using sonic anemometers at 7 m and hub height at 109 m which can be used to evaluate the turbulence integral length scale which should be representative of $L$. There are also temperature sensors at these locations. During the time of the present measurements, it is estimated as $L \approx 10\,\text{m}$ at 7 m height, and $L \approx 50\,\text{m}$ at hub height. Temperature is also measured at the above locations. The refractive index variance can be approximated using the following formula [1]:

$$\langle \mu^2 \rangle = \left( \frac{\sigma_v}{C_0} \right)^2 + \left( \frac{\sigma_T}{2\,T_0} \right)^2$$

where $C_0$ is the speed of sound and $T_0$ the average temperature, and $\sigma_v^2$ and $\sigma_T^2$ are the velocity and temperature variances, respectively. A rough estimate of the refractive index variance using the measurement data is $\langle \mu^2 \rangle = 10 \times 10^{-6}$. For comparison, the value $\langle \mu^2 \rangle = 1 \times 10^{-6}$ is also used in the figure discussed below.

The various combinations of the two parameter values (i.e. for $L$ and $\langle \mu^2 \rangle$) as input to the separation length as in Eq. (4) are plotted as curves against the measured log-amplitude variances in Fig. 11. It can be seen that the general trend of the saturation length decreasing with increasing frequency is also observed in the measurements. However, the decrease predicted by the theoretical formula appear to be faster towards high frequencies than the behaviour of the measuremed log-amplitude variances suggests. Furthermore, the value of $\langle \mu^2 \rangle = 10 \times 10^{-6}$ estimated from the measurement data appears too large as a better agreement is found using the value $\langle \mu^2 \rangle = 1 \times 10^{-6}$ instead.

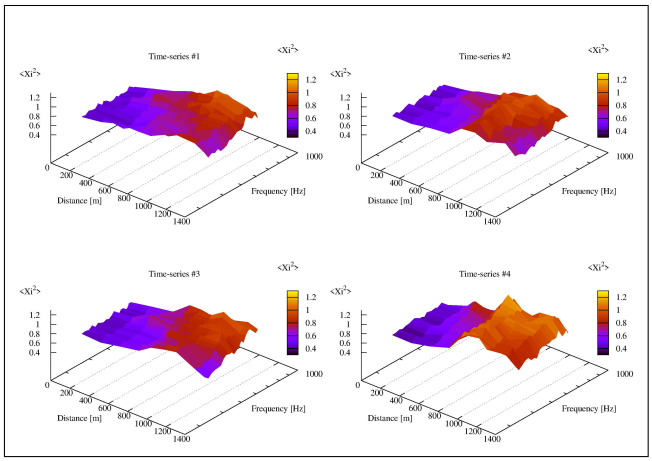


**Figure 10**. Log-amplitude variance for 500 Hz 1/1 octave band emission for the 4 individual sub-series used to calculate the same quantity in Fig. 7.

## 5. CONCLUSIONS

Noise measurements acquired with microphones located up to 1278 m at 1.5 m above the ground from a loudspeaker noise source which is located at 109 m height are analyzed. The log-amplitude and phase fluctuations are calculated when the loudspeaker is activated. These results are compared with a theoretical work on noise propagation for tonal noise in a turbulent medium assuming spherical waves. This theory yields the existence of a saturation length for the log-amplitude fluctuations which is also observed in the present measurement data. Nevertheless, there exist large discrepencies for the quantitative results, even though the general trend is reproduced.

There may be several explanations for the observed quantitative discrepancies. The theoretical formula used to evaluate saturation length is based on spherical sound waves. Thus, the reflections inherent to the present experimental set-up may have an impact on the saturation effect. The theory is also developed for a purely tonal noise source while broadband noise is used as a source in the present experiment, which may also have an impact when comparing the two approaches. An advanced noise propagation model (such as Parabolic Equations) combined with a model for atmospheric turbulence (such as Large Eddy Simulation) may help explain the above discrepancies.

The present study raises more questions than it answers. The actual experimental conditions of these measurements, including reflections and broadband noise, should be included in the theoretical approach, if such exists, to better understand the discrepancies.

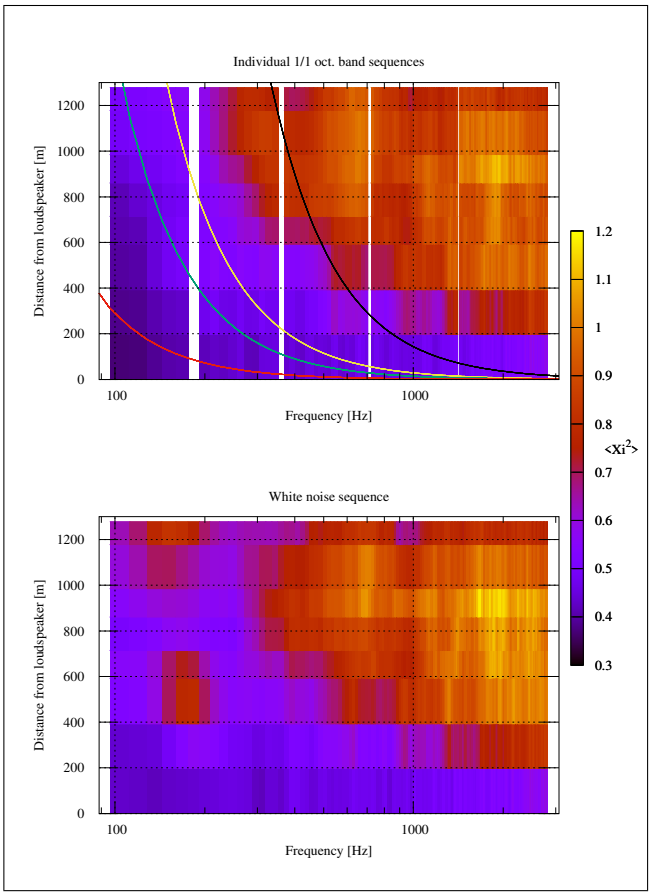


**Figure 11**. Log-amplitude variance for all 1/1 oct. band sequences (up) together with saturation length, and Log-amplitude variance for larger frequency band (down) (Curves on the upper plot are $r_s$ according to Eq. (4) - Black: $\langle \mu^2 \rangle = 1 \times 10^{-6}$ and $L = 10\,\mathrm{m}$, Yellow: $\langle \mu^2 \rangle = 1 \times 10^{-6}$ and $L = 50\,\mathrm{m}$, Blue: $\langle \mu^2 \rangle = 10 \times 10^{-6}$ and $L = 10\,\mathrm{m}$, Red: $\langle \mu^2 \rangle = 10 \times 10^{-6}$ and $L = 50\,\mathrm{m}$).

## 6. REFERENCES


[1] G. A. Daigle, J. E. Piercy, and T. F. W. Embleton, "Line-of-sight propagation through atmospheric turbulence near the ground," *J. Acoust. Soc. Am.*, vol. 74, no. 5, pp. 1505–1513, 1983.

[2] F. Rietdijk, F. Forssén, and K. Heutschi, "Generating sequences of acoustic scintillations," *Acta Acustica united with Acustica*, vol. 103, pp. 331–338, 2017.

[3] A. R. Wenzel, "Saturation effects associated with sound propagation in a turbulent medium," *Prog. Astronaut. Aeronaut.*, vol. 46, pp. 67–75, 1976.